Exp Fluids (2012) 53:467–480
DOI 10.1007/s00348-012-1302-8

RESEARCH ARTICLE

Synthetic jet control of separation in the flow over a circular cylinder

Li-Hao Feng · Jin-Jun Wang

Received: 14 June 2011 / Revised: 18 January 2012 / Accepted: 29 March 2012 / Published online: 13 April 2012

Abstract A synthetic jet generated by a non-sinusoidal waveform is used to control flow separation around a circular cylinder at Reynolds number 950. The synthetic jet is positioned at the rear stagnation point. The suction duty cycle factor defined as the ratio of the time duration of the suction cycle to the blowing cycle is introduced as the determining parameter. Increasing the suction duty cycle factor, the exit velocity and entrainment effect of the synthetic jet are enhanced, flow separation is delayed, and drag reduction by up to 29 % is achieved. Different mechanisms for separation control during both the blowing cycle and the suction cycle have been revealed. It is suggested that a better control effect can be obtained during the blowing cycle.

1 Introduction

As a kind of vortex ring control technique, synthetic jet has attracted much attention due to its unique advantages (Toyoda and Hiramoto 2009). It has been widely applied in various fields, including modification of the aerodynamic characteristics of bluff bodies, control of lift, and drag on airfoils and aircrafts, reduction of skin friction of a flat-plate boundary layer, mixing in circular jets, and control of internal flow separation and of cavity oscillations (Glezer and Amitay 2002; Zhang et al. 2008).

Amitay et al. (1997, 1998) applied the synthetic jet to control the boundary layer separation of a circular cylinder. They indicated that the interaction of synthetic jets with an embedding flow led to the formation of closed recirculation regions, which enabled an apparent modification of the flow boundary. Surface pressure measurement demonstrated that the synthetic jets could substantially reduce drag by up to 30 %. Hot-wire measurement indicated that the velocity fluctuations and Reynolds stress were all reduced at $x/D = 3$ with the synthetic jets positioned at 60°. Many other investigations have also proved that the synthetic jet can efficiently delay separation of flow around a circular cylinder, make the separation region diminish or even completely disappear, and lead to a drag reduction and a resonant response decrease (Crook et al. 1999; Rediniotis et al. 1999; Béra et al. 2000; Tensi et al. 2002; Fujisawa and Takeda 2003; Glezer et al. 2003; Wolfe and Ziada 2003; Fujisawa et al. 2004; Wang et al. 2007; Feng et al. 2008). Recent investigations indicated that the synthetic jet could also change the wake vortex shedding mode (Feng and Wang 2010; Feng et al. 2010, 2011).

Among these investigations, the synthetic jet was usually positioned near the separation point. However, Amitay et al. (1997) and Feng et al. (2008) all concluded that the synthetic jet positioned at the rear stagnation point could also delay flow separation. There are some other control techniques based on the rear stagnation point, such as base bleed and splitter plate. Tan et al. (2001), Fu and Rockwell (2005) and Baek and Karniadakis (2009) found that the base bleed could change the cylinder wake. Hwang et al. (2003), Mittal (2003), and Akilli et al. (2005, 2008) indicated that a splitter plate attached to the rear stagnation point or inside the wake region could partly or completely suppress the vortex shedding and even reduce the drag force and lift fluctuation.

It is also required to increase the efficiency of the synthetic jet for flow control. Based on the theoretical jet

L.-H. Feng · J.-J. Wang (✉)
Fluid Mechanics Key Laboratory of Education Ministry,
Beijing University of Aeronautics and Astronautics,
Beijing 100191, People's Republic of China
e-mail: jjwang@buaa.edu.cn

formation criterion suggested by Holman et al. (2005), Zhang and Wang (2007) proposed a novel actuator signal based on a non-sinusoidal waveform to generate a more efficient synthetic jet. This non-sinusoidal waveform can be obtained by changing the ratio of the suction cycle to the blowing cycle, which is defined as the suction duty cycle factor k, while keeping the mass flux and generation cycle unchanged. Based on the numerical simulation, Zhang and Wang (2007) proved that the entrainment effect of the synthetic jet increased with the suction duty cycle factor, so that the synthetic jet could propagate farther downstream and coalesce to synthesize a stronger vortex pair. Toyoda and Hiramoto (2009) also appraised the effect of the non-sinusoidal waveform in their review. Shan and Wang (2010) and Wang et al. (2010) experimentally validated that using the non-sinusoidal waveform could enhance the strength of an axisymmetric synthetic jet vortex ring and a two-dimensional synthetic jet vortex pair in a quiescent fluid, respectively. Feng et al. (2008) found that the control effect of the synthetic jet on flow around a circular cylinder was enhanced by increasing the suction duty cycle factor based on the flow visualization experiment.

For application of the non-sinusoidal synthetic jet to control flow around a circular cylinder, our previous work (Feng et al. 2010) has studied the vortex dynamics with the synthetic jet positioned at the rear stagnation point. It was found that this control configuration could lead to three kinds of vortex patterns: for $k = 0.25, C_\mu = 0.148$, where C_μ is the equivalent momentum coefficient based on the synthetic jet blowing velocity averaged only in the blowing cycle (detail definition can be found in Sect. 2.1), vortex synchronization at the subharmonic excitation frequency with antisymmetric shedding mode; for $0.50 \le k \le 1.00, 0.213 \le C_\mu \le 0.378$, vortex synchronization at the excitation frequency with the symmetric or antisymmetric shedding modes; and for $2.00 \le k \le 4.00$, $0.850 \le C_\mu \le 2.362$, vortex synchronization at the excitation frequency with symmetric shedding mode. The occurrence of the symmetric mode has a significant influence in practical applications, and it will consequently result in a significant variation for the flow field. As a subsequent study, therefore, this paper pays particular attention on the separation control as well as drag reduction associated with the aforementioned variations in the vortex shedding mode.

2 Experimental setup

2.1 Experimental model

The synthetic jet actuator system comprised a computer, an A/D conversion card, a programmable logic controller (PLC), a servo electromotor, and a center-setting crank mechanism that was formed by an eccentric disk and a connecting rod, a piston, and an "L"-shape hollow cylinder, as shown in Fig. 1. More details about this system can refer to the related papers (Wang et al. 2007; Feng et al. 2010). Briefly, the non-sinusoidal waveform could be programmed in the computer, and then, it controlled the actuator to generate the so-called novel synthetic jet (Zhang and Wang 2007). The generation cycle and exit velocity of the synthetic jet were altered by adjusting the excitation amplitude A (the maximum displacement of the piston to the zero position), the excitation frequency f_e, and the suction duty cycle factor k.

The experimental model was the horizontal section of the "L"-shape hollow cylinder with outer diameter $D = 30$ mm, inner diameter $d = 22$ mm, and length 600 mm. End plates were used in order to maintain the two dimensionality of the flow field with their distance of 500 mm. The cylinder was 300 mm from the leading edge of end plates. A slot was placed at the rear stagnation point of the circular cylinder, namely 180° from the front stagnation point. In order to ensure a well-developed

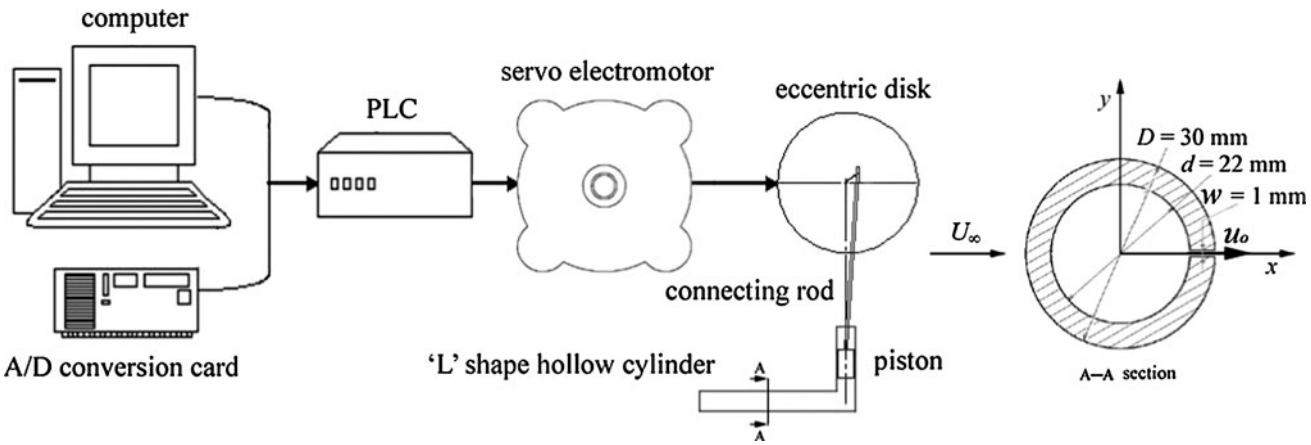

Fig. 1 Synthetic jet actuator system (Feng et al. 2010)

2-D synthetic jet flow, the slot length was selected as $l = 50$ mm with its width $w = 1$ mm. Since the present work focused on the very-near-wake region of the cylinder in the mid-span of the slot, the slot ends of the synthetic jet did not affect the flow of the test section greatly. This has been confirmed in the previous work by Feng et al. (2008).

The experiment was conducted in a recirculation water channel. The size of the test section is 600 × 600 × 4,800 mm, and the streamwise turbulence intensity is no more than 0.8 %. Based on the previous investigations (Feng and Wang 2010; Feng et al. 2010, 2011), the free-stream velocity was selected at $U_\infty = 41.8$ mm/s, corresponding to the circular cylinder Reynolds number $Re = 950$. The natural shedding frequency was 0.30 Hz, giving $St = 0.215$. A series of experiments indicated that the strength of the synthetic jet vortex pair was a more important factor rather than the normalized excitation frequency (Feng and Wang 2010; Feng et al. 2011). Using the standard sinusoidal waveform, Feng et al. (2011) found that the control case at the excitation amplitude $A = 5.5$ mm and the excitation frequency $f_e = 0.50$ Hz was under a bi-stable state, where the vortex shedding varied between the symmetric and antisymmetric ones. Increasing or decreasing the excitation frequency could result in the complete symmetric mode or the original antisymmetric mode. Thus, the present study followed these excitation parameters, while the suction duty cycle factor k was selected at 0.25, 0.50, 1.00, 2.00, and 4.00, aimed at further enhancing the control effect using the non-sinusoidal waveform. It gave the equivalent momentum coefficient $C_\mu = 0.148$, 0.213, 0.378, 0.850, and 2.362, respectively. Here, the momentum coefficient is defined as

$$C_\mu = 2\left(\frac{\overline{U_b}}{U_\infty}\right)^2\left(\frac{w}{D}\right), \tag{1}$$

where $\overline{U_b}$ is the blowing velocity averaged only in the blowing cycle. It can be deduced based on mass conservation ignoring viscous effects:

$$\overline{U_b} = \frac{(k+1)\pi D_p^2 A f_e}{2lw}, \tag{2}$$

where $D_p = 24$ mm is the outer diameter of the piston. Detail information about the exit velocity can be found elsewhere (Feng et al. 2010). The origin of the coordinate system is located at the center of the experimental cylinder, while the x- and y-axis represent the streamwise and vertical directions, respectively.

2.2 Velocity measurement

The flow around the circular cylinder was measured by PIV technique. The field of view was illuminated by a light sheet from an Nd/YAG continuous laser. It was captured by a CCD camera with spatial resolution of 640 × 480 pixels and gray level of 8 bits. The field of view for the very-near-wake region had a range of $0 \le x/D \le 3$ and $-1 \le y/D \le 1$, while another view of $2.5 \le x/D \le 5.5$ and $-1 \le y/D \le 1$ was also measured for drag estimation. The sampling frequency was 100 Hz (temporal resolution 0.01 s) with the exposure time 5 ms. Ten thousands frames were recorded continuously in one case, namely 50 cycles of vortex shedding for each control case.

The commercial software MicroVec 2.0 was used to calculate the velocity and vorticity fields. The images were analyzed based on the cross-correlation algorithm between two successive images. The gray-level difference method was used to deal with particle images, which helped to simultaneously promote the signal-to-noise ratio. Gaussian peak fit was applied to enhance the resolution of cross-correlation peak identification to a subpixel level. The sizes of the interrogation window and search window were 16 × 16 pixels and 8 × 8 pixels, respectively. The spatial resolution was approximately 1.1 mm in both streamwise and vertical directions, giving 4,256 vectors for each snapshot. Multi-grid iteration with window deformation was also used to improve the trace accuracy of the interrogation window. Time-averaged quantities were calculated from 10,000 PIV snapshots, while phase-averaged quantities were calculated from about 50 cycles. Statistical analysis for the velocities and their fluctuations at $x/D = 0.7$ and $y/D = 0$ has indicated that the time-averaged or phase-averaged velocity components and their fluctuations start to show a satisfactory convergence after approximately 3,000 snapshots or 15 cycles. The uncertainty of the velocity measurement was better than 2 mm/s according to Feng and Wang (2010).

3 Results and discussion

3.1 Time-averaged flow field

Figure 2 shows contours of the time-averaged speed $\sqrt{U^2+V^2}/U_\infty$ superposed with velocity vector for the natural and control cases to present an overall control effect. There exists a velocity defect region where backflow is obvious in the near wake for the natural case, forming a large-scale recirculation region (Fig. 2a). When the synthetic jet is actuated (Fig. 2b–f), it injects high-speed fluid into the near-wake region from the rear stagnation point. The streamwise velocity near the rear stagnation point increases, and the velocity defect decreases with the suction duty cycle factor. The backflow has nearly disappeared for $k \ge 2.00$. Meanwhile, the flow topology in the

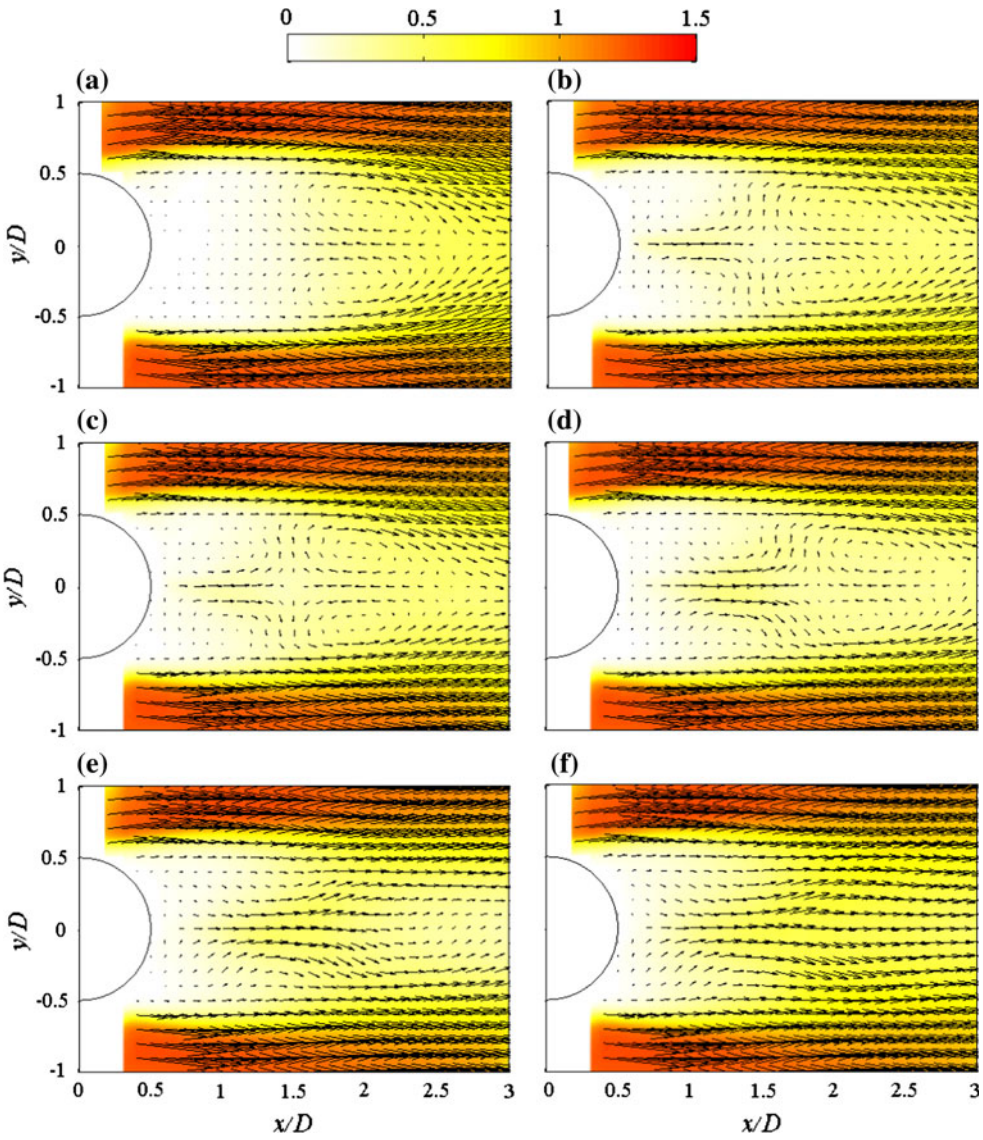

Fig. 2 Time-averaged speed $\sqrt{U^2 + V^2}/U_\infty$ superposed with velocity vector. **a** Natural case, **b** $k = 0.25$, **c** 0.50, **d** 1.00, **e** 2.00, **f** 4.00

near-wake region is also changed. For $k \leq 1.00$ (Fig. 2b–d), two recirculation regions form at upstream and downstream of the wake region, respectively. The upstream recirculation region is induced by the periodic blowing and suction, while the downstream recirculation region is induced by the inherent separation of flow around the cylinder. The downstream recirculation region is smaller than the natural case due to the formation and compression of the upstream recirculation region. Such variations are similar with Fu and Rockwell (2005) and Baek and Karniadakis (2009), who controlled the circular cylinder by means of base bleed and also observed two recirculation regions in the near-wake region. For $k = 2.00$ and $k = 4.00$ (Fig. 2e, f), the synthetic jet exit velocity is increased greatly, so that the recirculation region disappears and it exhibits a jet-alike flow field.

The decrease in the recirculation region size suggests a delay in flow separation around the circular cylinder, which can be further validated from the distributions of the time-averaged tangential velocity shown in Fig. 3. The velocity profile shows a defect from 150° for the natural case. It becomes much fuller for all the control cases in the near-wall region, suggesting that the flow around the circular cylinder is more resistant to separate. Away from the cylinder surface, the tangential velocity increases with the suction duty cycle factor.

The synthetic jet can induce a localized jet flow around the centerline in the near-wake region, which is clearly seen in Fig. 4. According to Rumsey et al. (2004), the distance between two positions where the value is half of the sum of the local maximum and minimum values can be considered as the jet width b. Thus, inside such control

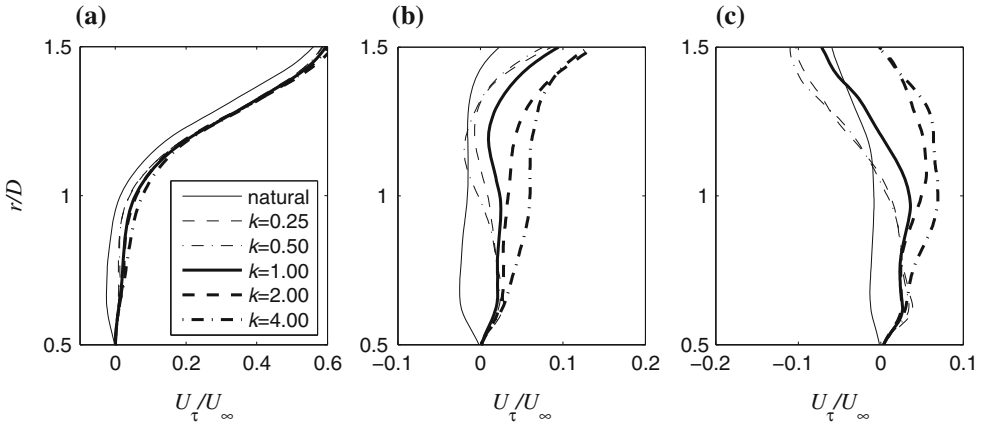

Fig. 3 Time-averaged tangential velocity profile at different azimuth angles along the radius of the circular cylinder. **a** 150°, **b** 160°, **c** 170°

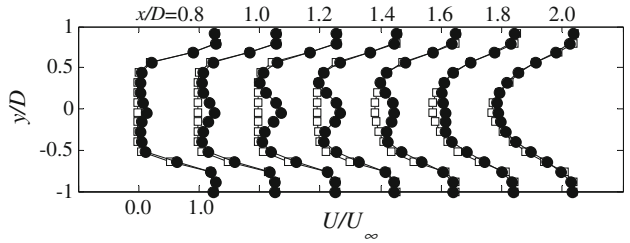

Fig. 4 Distributions of time-averaged streamwise velocity U/U_∞ for natural case (*open square*) and $k = 1.00$ (*filled square*)

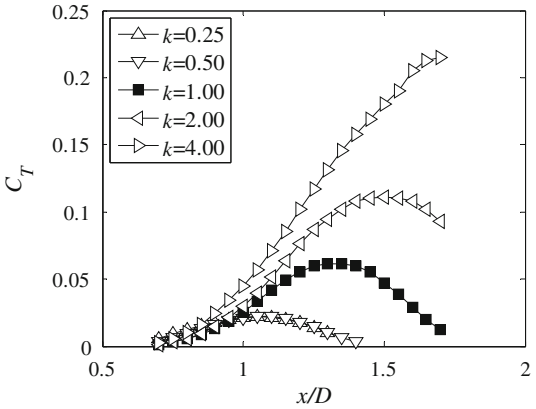

Fig. 5 Time-averaged thrust coefficient introduced by the synthetic jet

volume within b, the time-averaged momentum flux per unit spanwise length M,

$$M = \int_{-b/2}^{b/2} \rho(UU + \overline{u'u'})\,\mathrm{d}y, \tag{3}$$

can be calculated, with the assumption that the static pressure within the jet is streamwise invariant (Smith and Glezer 1998; Spall et al. 2004; Yannopoulos 2006). When the synthetic jet injects high-speed fluid into the near-wake region, it also generates a thrust. The direction is opposite to the inherent drag force. Based on the momentum theory, the jet-induced thrust force T/unit spanwise length is equal to the momentum flux M, giving $T = M$ (Jukes and Choi 2009a). Here, the thrust force is normalized by the dynamic pressure $0.5\rho U_\infty^2 D$, giving the thrust coefficient C_T induced by the synthetic jet

$$C_T = M/\left(0.5\rho U_\infty^2 D\right). \tag{4}$$

The mean thrust coefficients for different suction duty cycle factors are compared in Fig. 5. In general, the thrust coefficient increases with the x-axis until a peak value and then decreases as the synthetic jet is convected downstream, indicating the strong entrainment ability of the vortex pair by enhancing the momentum mixing. Another important suggestion is that the thrust coefficient increases with the suction duty cycle factor.

Figure 6 further illustrates maximum thrust generation rate by the synthetic jet in the form of momentum coefficient. It is shown that the conversion efficiency from synthetic jet to thrust is relatively low, which is only in the range 0.09–0.16. This is mainly suffered from two effects: the present control configuration and the existence

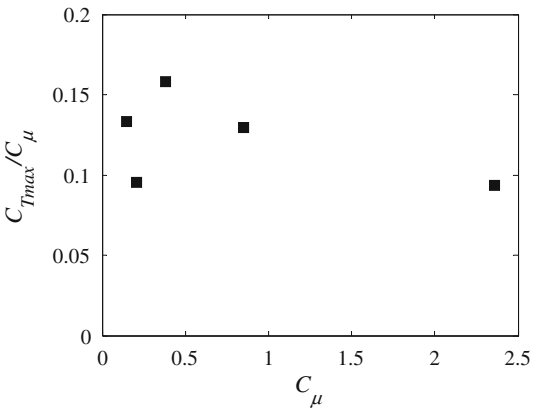

Fig. 6 Maximum thrust generation efficiency versus momentum coefficient

of the suction cycle. Since the synthetic jet is positioned at the rear stagnation point, when the synthetic jet vortex pair is induced and convected downstream into the recirculation region, it will be weakened by the backward flow, as has been pointed out by Feng and Wang (2010) and Feng et al. (2010, 2011). Besides, the suction process of the synthetic jet also affects the blowing velocity. Consequently, these two factors reduce the localized jet velocity shown in Fig. 4 as well as its integral value shown in Fig. 5.

3.2 Drag estimation

The measurement of unsteady force on a circular cylinder is an interesting issue. In general, the fluid forces are usually obtained by force balance measurement or integrating the pressure distributions around the cylinder. Although these techniques can provide accurate measurement of fluid forces, they also need an elaborate experimental test equipment and test model, which are often very difficult to construct in some situations (Fujisawa et al. 2005). Consequently, many researchers have strived to calculate the forces on the bluff body by velocity measurement, which are usually based on Navier–Stokes equations (van Dam 1999). According to Antonia and Rajagopalan (1990), the mean drag coefficient C_D of a circular cylinder could be estimated from the wake profile of the mean velocity and Reynolds stress field using the following equation:

$$C_{\mathrm{D}} = 2\int_{-\infty}^{\infty}\frac{U}{U_\infty}\left(1-\frac{U}{U_\infty}\right)d\left(\frac{y}{D}\right)+2\int_{-\infty}^{\infty}\left(\frac{\overline{v'v'}-\overline{u'u'}}{U_\infty^2}\right)d\left(\frac{y}{D}\right) \tag{5}$$

As shown by Eq. (5), that C_D can be divided into two components. The first component on the right-hand side is determined by the streamwise velocity, termed as I_1, while the second component corresponds to the contribution of the Reynolds stress, termed as I_2. Although the drag coefficient can also be calculated only by term I_1, it requires that the velocity profile is measured at a relatively large value of x/D. Thus, term I_2 is supplied to correct the drag prediction in case that the measured velocity is not so far away enough. Antonia and Rajagopalan (1990) indicated that the computed drag coefficient by Eq. (5) was in the range of the published literature of Zdravkovich (1997). In the following studies, So et al. (2000), Lam et al. (2004), Zhang et al. (2004), Konstantinidis and Balabani (2007), and Zhou et al. (2011) all indicated the rationality of using Antonia and Rajagopalan's (1990) method to estimate the drag coefficient of a circular cylinder or an airfoil.

In this study, drag coefficients calculated at $x/D = 5.5$ and $-1 \le y/D \le 1$ are adopted for a relative comparison. For the natural case, C_{D0} is estimated as 1.0 based on the present PIV data. The drag coefficient of a natural circular cylinder around $Re = 1{,}000$ is about 0.97–1.01 and 1.00 according to the summarized data from Cantwell and Coles (1983) and Zdravkovich (1997), respectively. Therefore, the present drag coefficient estimation is reasonable, which has an uncertainty <3 %. Although the drag prediction is not completely accurate for all cases, at least, it can provide us a relative comparison.

Figure 7a presents characteristics of C_D, I_1 and I_2 for different cases, which have been normalized by C_{D0}. It is shown that the drag reduction is more significant with an increase in the suction duty cycle factor, namely the momentum coefficient. This agrees well with the finding that the flow separation is delayed with the suction duty cycle factor in Fig. 3. Besides, the thrust force produced by the synthetic jet could counteract the drag force in some extent. The maximum thrust coefficients normalized by C_{D0} are about 2, 2, 6, 11, and 22 %, corresponding to the drag reduction appropriately 12, 13, 17, 24, and 29 % for the suction duty cycle factor varying from $k = 0.25$ to $k = 4.00$, respectively. However, the component I_1 for the control cases has nearly no change or even has a small increment in comparison with the natural case, while the component I_2 is reduced significantly as k increases. Hence, it is suggested that the drag reduction can be primarily achieved by a decrease in the Reynolds stress component. The present drag reduction is consistent with previous studies, such as Amitay et al. (1997) and Fujisawa and Takeda (2003), who all obtained a considerable drag reduction by up to 30 %. Figure 7b indicates that the contribution of the component I_1 to the total drag coefficient is more significant than that of the component I_2. The component I_1/C_D increases with the suction duty cycle factor, while the component I_2/C_D decreases with it.

From the above analysis, it seems that the primary essential of drag reduction is due to the decrease in the Reynolds stress component ($\overline{v'v'} - \overline{u'u'}$). This is consistent with the formation of the symmetric wake vortex shedding mode at larger suction duty cycle factors, since the symmetric modes can significantly reduce the mutual interaction between upper and lower wake vortices (Feng et al. 2010), which is considered as a main source of Reynolds stress generation. Whereas, since the component I_2 occupies less proportion to the total drag coefficient than the component I_1 and it just reaches up to a maximum of about 32 % for the natural case, the decrease of I_2 may only lead to a total drag reduction by up to 30 %, which has been exhibited by the control case $k = 4.00$. Thus, in order to achieve a much more remarkable drag reduction, the

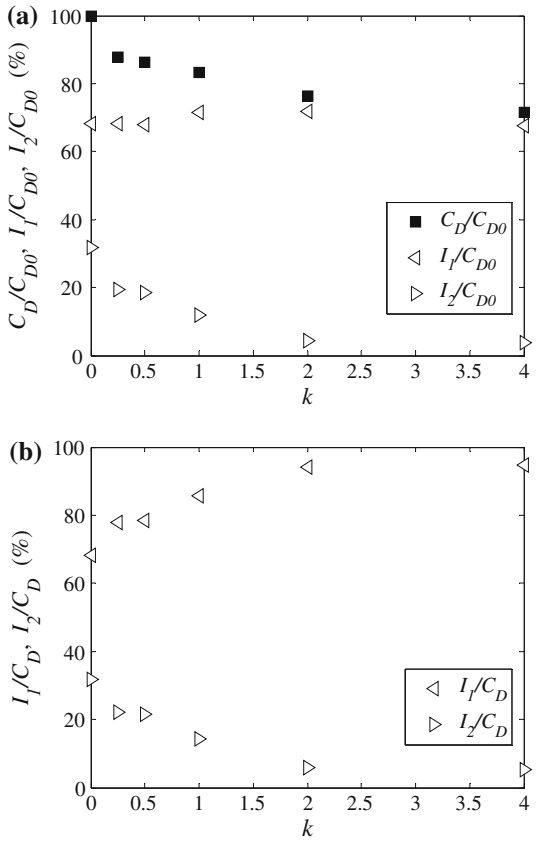

Fig. 7 Variations of the drag coefficient **a** and the contributions of I_1 and I_2 to total drag coefficient **b**

component I_1 should be further reduced, suggesting that the streamwise velocity in the wake region needs to be more uniform.

The drag reduction efficiency by the present synthetic jet is further analyzed in Fig. 8. The control efficiency on drag reduction decreases with the momentum coefficient, though the absolute drag reduction increases with it. The minimum drag reduction efficiency is only about 0.12/momentum coefficient at the largest momentum coefficient

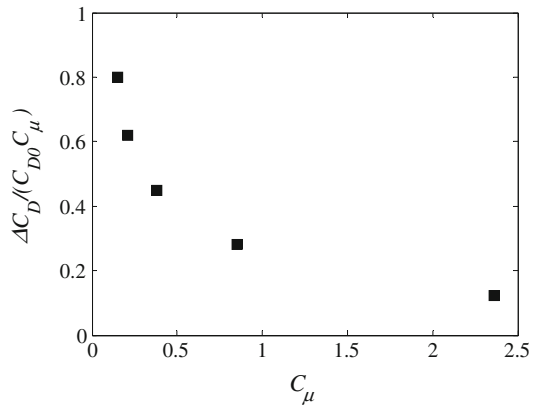

Fig. 8 Drag reduction efficiency versus momentum coefficient

($k = 4.00$). Thus, it is suggested that the present control configuration is a rather inefficient strategy when considering the consumed power, which is mainly due the position of the synthetic jet. It is placed at the rear stagnation point other than more sensitive positions, namely around the separation point. Thus, the synthetic jet vortex pair needs more energy to be strong enough to avoid being attenuated in the recirculation region. However, in addition to the drag reduction, the present method has the potential application in reducing the vortex-induced vibration by inducing the symmetric vortex shedding mode (Feng and Wang 2010; Feng et al. 2010, 2011). In order to obtain a more efficient control way, it is better to take full advantage of the "frequency" characteristic of the synthetic jet by placing it around the separation point rather than based on the vortex strength by placing it at the rear stagnation point (Jukes and Choi 2009b).

3.3 Phase-averaged flow field

From the above analysis, it is indicated that varying the suction duty cycle factor (momentum coefficient) results in an apparent difference in the control effect. Thus, detailed information of the flow field during one cycle is studied in this section to interpret the separation delay and drag reduction. The phase-average method is similar with Kim et al. (2006) and Zhou and Yiu's (2006). Close-up view of the phase-averaged velocity vector just near the leeward side of the circular cylinder is shown in Fig. 9. Since the power spectrum analysis suggests that the near-wake flow field around the cylinder is synchronized by the synthetic jet, the phase-averaged results in present field of view can well exhibit the process of flow separation control during one cycle. Four typical phases are selected for comparison, which are the start of the blowing cycle ($\Phi = 0°$), middle of the blowing cycle ($\Phi = 90°$), start of the suction cycle ($\Phi = 180°$), and middle of the suction cycle ($\Phi = 270°$), corresponding to the four columns from left to right in Fig. 9.

When adopting the standard sinusoidal actuator signal (Fig. 9c), it is shown that better control effect is achieved at the middle of both the blowing cycle and suction cycle. The large-scale recirculation region disappears and small-scale separation bubble forms near 140°. However, the patterns of the velocity vector at these two phases are different. At the middle of the blowing cycle, the fluid flows toward the centerline near the jet exit and then downstream, whereas at the middle of the suction cycle, the flow is upstream toward the jet exit. In comparison, the control effect at the start of the blowing or suction cycles is not so significant.

When decreasing the suction duty cycle factor to $k = 0.25$ and $k = 0.50$ (Fig. 9a, b), the blowing velocity of

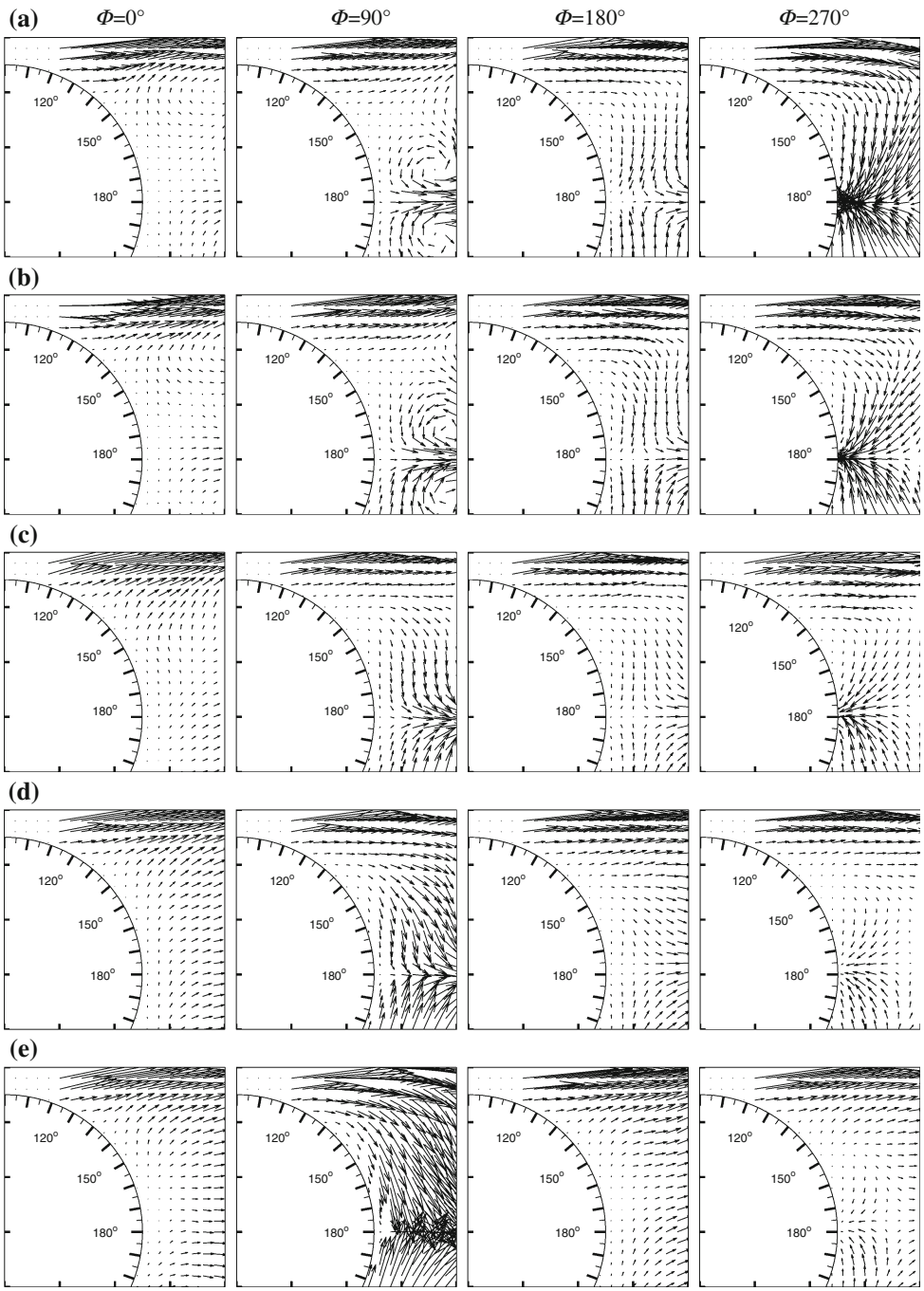

Fig. 9 Close-up view of the phase-averaged velocity vector in the near-wake region showing the effect of synthetic jet on separation control of the circular cylinder. The x-axis is from $x/D = 0$ to $x/D = 0.8$, and the y-axis is from $y/D = -0.2$ to $y/D = 0.6$. **a** $k = 0.25$, **b** 0.50, **c** 1.00, **d** 2.00, **e** 4.00

the synthetic jet is reduced, while the suction velocity is enhanced. Therefore, the flow separation is not delayed so much during the blowing cycle, while the separation region is reduced significantly during the suction cycle. It is noteworthy that the flow around the circular cylinder is nearly attached at the middle of the suction cycle for $k = 0.25$, exhibiting that the velocity vectors around the circular cylinder are all pointing to the rear stagnation point.

In comparison, when increasing the suction duty cycle factor to $k = 2.00$ and $k = 4.00$ (Fig. 9d, e), the blowing velocity of the synthetic jet is enhanced significantly, while the suction velocity is reduced. The optimal control effect is achieved at the middle of the blowing cycle. It is shown that flow separation is evidently delayed at this time for $k = 2.00$, while it is completely eliminated for $k = 4.00$. However, the flow separation state does not change very much during the suction cycle.

It is indicated that the optimal separation control effect is achieved at the middle of the suction cycle for $k < 1.00$ and at the middle of the blowing cycle for $k > 1.00$, respectively. These typical control cases are further

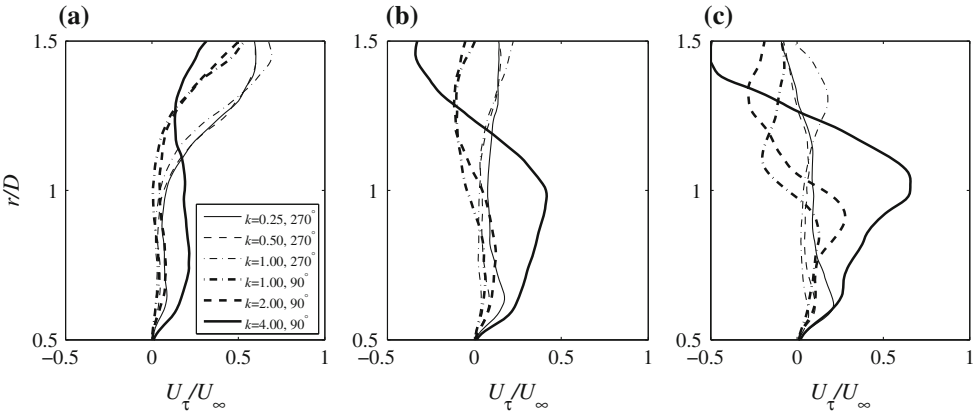

Fig. 10 Phase-averaged tangential velocity profile at different azimuth angles along the radius of the circular cylinder at the middle of the suction cycle for $k \leq 1.00$ and at the middle of the blowing cycle for $k \geq 1.00$. **a** 150°, **b** 160°, **c** 170°

compared in Fig. 10. Note that in theory, the suction velocity at the exit for $k = 0.25$, 0.50, and 1.00 is equivalent to the blowing velocity for $k = 4.00$, 2.00, and 1.00, respectively. However, it is suggested that the blowing process of the synthetic jet obtains a better control effect than the suction process, since the velocity profile near the wall region becomes much fuller for the former case.

The different control effects between the blowing cycle and suction cycle are examined by comparing the entrainment ability of the synthetic jet. According to Grinstein (2001) and Toyoda and Hiramoto (2009), the entrainment effect of the vortex pair can be evaluated by calculating the mass flux Q

$$Q = \int_{-b/2}^{b/2} \rho U \mathrm{d}y. \tag{6}$$

Here, the mass flux is normalized by $\rho U_\infty D$, giving the mass flux coefficient C_Q. Figure 11 presents two typical control cases of $k = 0.50$ and $k = 2.00$ for several typical phases. From phase $\Phi = 0°$ to phase $\Phi = 360°$, the streamwise position of the maximum flux coefficient increases, since it has been shown by Feng et al. (2010) that the synthetic jet vortex pair is induced and converted downstream gradually, entraining surrounding fluids. The peak value occurs around the later half duration of the blowing cycle for both cases, and their values in the very-near-wake region are larger than other phases. When comparing the present results with the previous investigation by Feng et al. (2010), it further validates the important role of the vortex pair in the entrainment effect, since it was found that the large vortex recirculation also occurred around later half duration of the blowing cycle. Also note that the negative value occurs during the suction cycle for $k = 0.50$, showing the enhanced suction velocity by decreasing the suction duty cycle factor. However, the mass flux for $k = 2.00$ is much larger than that for $k = 0.50$, considering the same phase.

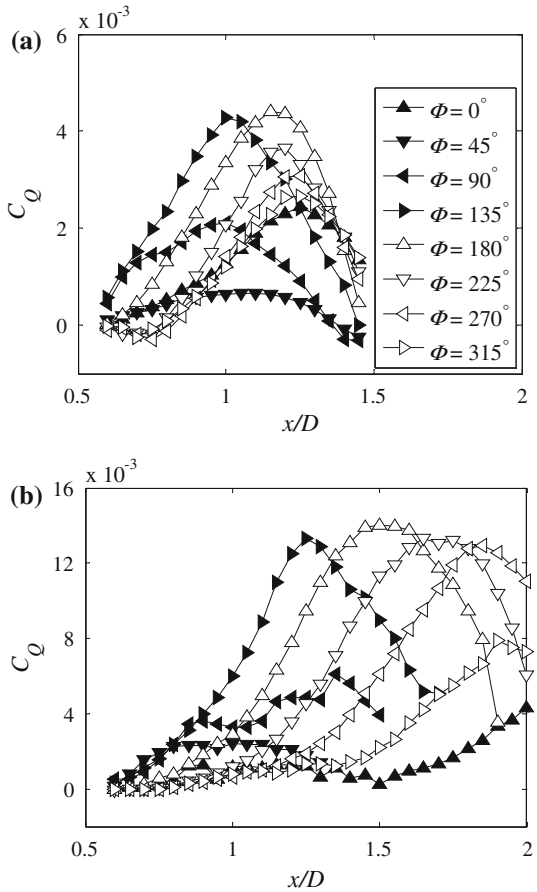

Fig. 11 Distribution of the mass flux coefficient for $k = 0.50$ (**a**) and $k = 2.00$ (**b**) at eight different phases

Figure 12 further compares the thrust coefficient for $k = 0.50$ and $k = 2.00$. The thrust coefficient increases during the blowing cycle and reaches the maximum value around the end of the blowing cycle. Then, it decreases during the suction cycle, and the peak position also moves further downstream. Increasing the suction duty cycle factor increases the thrust coefficient greatly, since it is shown that the maximum thrust coefficient is only about

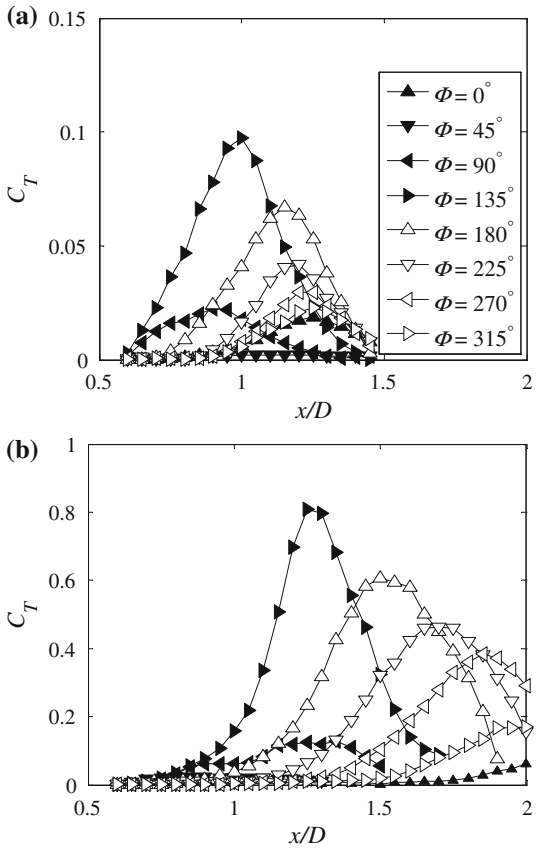

Fig. 12 Distribution of the thrust coefficient for $k = 0.50$ (**a**) and $k = 2.00$ (**b**) at eight different phases

0.1 for $k = 0.50$, while it can reach up to appropriately 0.8 for $k = 2.00$.

The strong entrainment of the vortex pair is thought to enhance the momentum mixing surrounding the circular cylinder. According to Benard et al. (2008), this can be inspected by showing the phase-averaged turbulent kinetic energy (TKE), $0.5\left(\overline{u'u'} + \overline{v'v'}\right)/U_\infty^2$ (see Fig. 13). When adopting the standard sinusoidal waveform, the blowing cycle and suction cycle produce comparable TKE. For $k = 0.25$ and $k = 0.50$, the suction process produces larger TKE than that produced by the blowing process, while the control cases of $k \geq 2.00$ result in an opposite distribution. In comparison with the continuous jet, one distinct advantage of the synthetic jet is that it can transport vortex pair into the outer flow, which enhances the turbulence mixing between inside of the separation region and the outer flow (Smith and Swift 2003). Thus, the fluids flowing over the circular cylinder can obtain high enough energy to overcome the adverse pressure gradient and viscous resistance to delay flow separation or reattach the separated flow. Consequently, the distributions of high-level TKE agree well with the separation control effect shown in Fig. 9.

As shown in Fig. 9, when the flow around the circular cylinder is attached, the vertical velocity near the upper leeward side is mainly negative. Thus, the negative vertical velocity gradient $((\partial v/\partial x)/(D/U_\infty))$ stands for the favorable pressure gradient and the flow acceleration toward the centerline, which is beneficial to flow separation delay. The opposite distributions of the vertical velocity or its gradient will accelerate flow separation. Due to the symmetry of the cylinder flow to its centerline, the following discussion is based on the upper leeward side. For all the control cases, the vertical velocity gradient at the start of the blowing cycle is nearly equal to zero or even to positive value, suggesting that the flow is ready to separate in this region, as shown from the first column in Fig. 14. At the middle of the blowing cycle (the second column in Fig. 14), the vertical velocity gradient near the cylinder leeward side becomes negative. The negative value is enhanced, and the influence region is enlarged as the suction duty cycle factor increases, indicating that the flow separation is delayed. At the start of the suction cycle (the third column in Fig. 14), the negative vertical velocity gradient decreases to nearly zero as the suction duty cycle factor increases. However, at the middle of the suction cycle (the last column in Fig. 14), the vertical velocity gradient becomes negative again, and both the negative value and its influence region are reduced with the suction duty cycle factor, suggesting that the optimal control effect is achieved for the smallest k case at this time, that is, $k = 0.25$. The variations of the vertical velocity gradient are in good agreement with the flow separation control results in Fig. 9.

4 Conclusions

Flow around a circular cylinder is controlled by a synthetic jet generated by a non-sinusoidal waveform. The synthetic jet is positioned at the rear stagnation point. PIV system is used to measure the velocity field at $Re = 950$. The suction duty cycle factor k defined as the ratio of the time duration of the suction cycle to the blowing cycle is introduced as the determining parameter.

When increasing the suction duty cycle factor, the exit velocity and the entrainment effect of the synthetic jet are enhanced. Thus, the velocity defect in the near-wake region is decreased, flow separation is delayed, and drag force is reduced. Phase-averaging analysis indicates that the synthetic jet can well control flow separation around a circular cylinder during both the blowing and suction cycles. However, the separation control mechanism during these two cycles is different. Flow separation can be delayed or eliminated by either injecting high-momentum fluid into the near-wake region during the blowing cycle or removing low-momentum fluid from the near-wake region during the

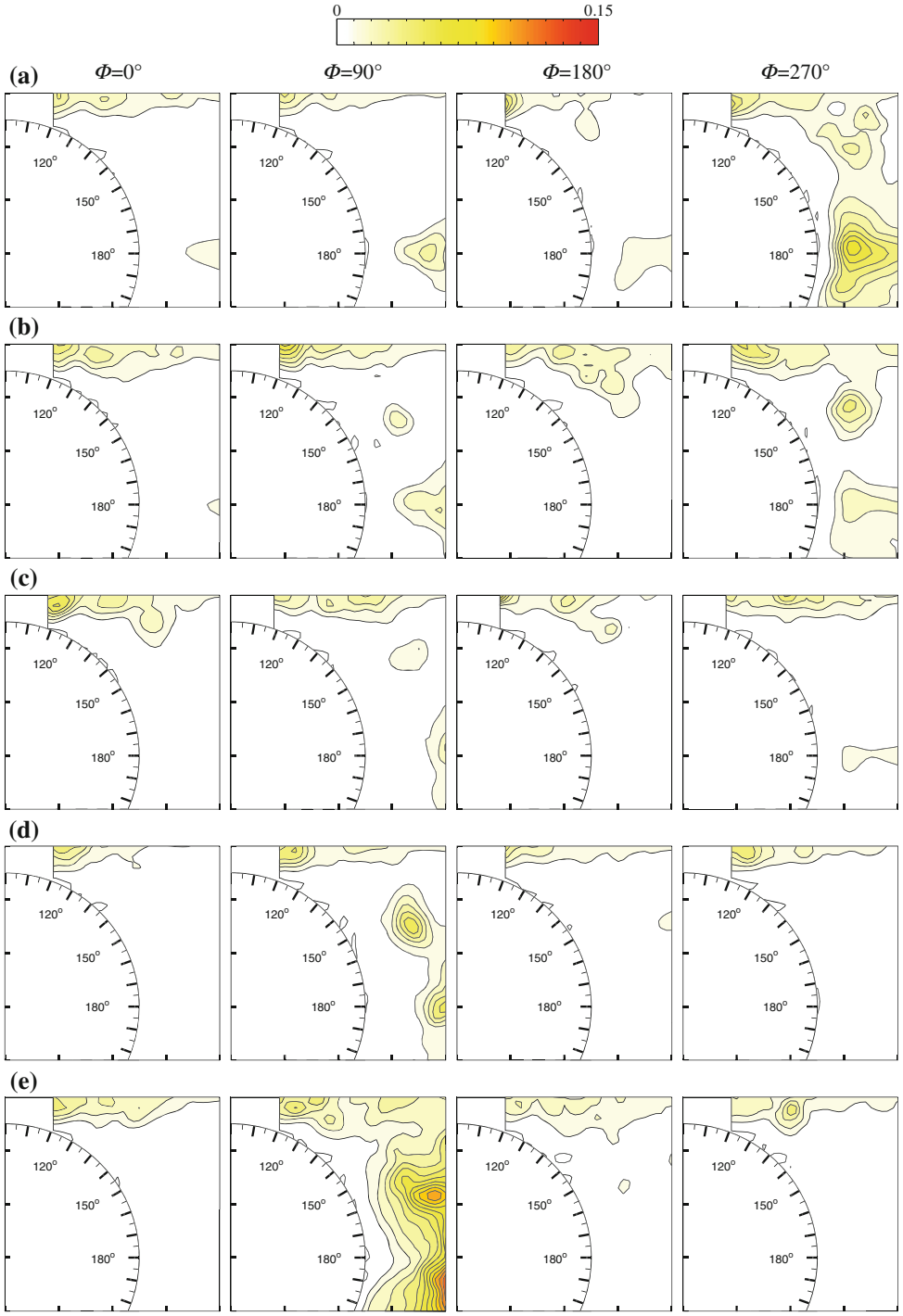

Fig. 13 Close-up view of the phase-averaged TKE in the near-wake region showing effect of synthetic jet on separation control of the circular cylinder. The x-axis is from $x/D = 0$ to $x/D = 0.8$, and the y-axis is from $y/D = -0.2$ to $y/D = 0.6$. **a** $k = 0.25$, **b** 0.50, **c** 1.00, **d** 2.00, **e** 4.00. Contour levels: 0.01

suction cycle, similar with the suggestion of Rediniotis et al. (1999). Moreover, the dominant features of vortex rings are the "entrainment" of the surrounding fluid and the "traveling" by self-induction (Toyoda and Hiramoto 2009), which are the same for the vortex pairs. The synthetic jet increases the TKE and enhances the momentum exchange of the flow field. Thus, accompanying with the synthetic jet control, there will be a vertical velocity acceleration pointing to the centerline, which is beneficial to separation delay. However, the blowing process of the synthetic jet obtains a better control effect than the suction process, considering the same blowing and suction velocity. This also accounts for the maximum drag reduction by up to 29 % at $k = 4.00$. However, the control efficiency on drag reduction is relatively low for the present control configuration, and it decreases with the suction duty cycle factor. In order to obtain a more efficient control result in drag reduction, it is better to place the synthetic jet around

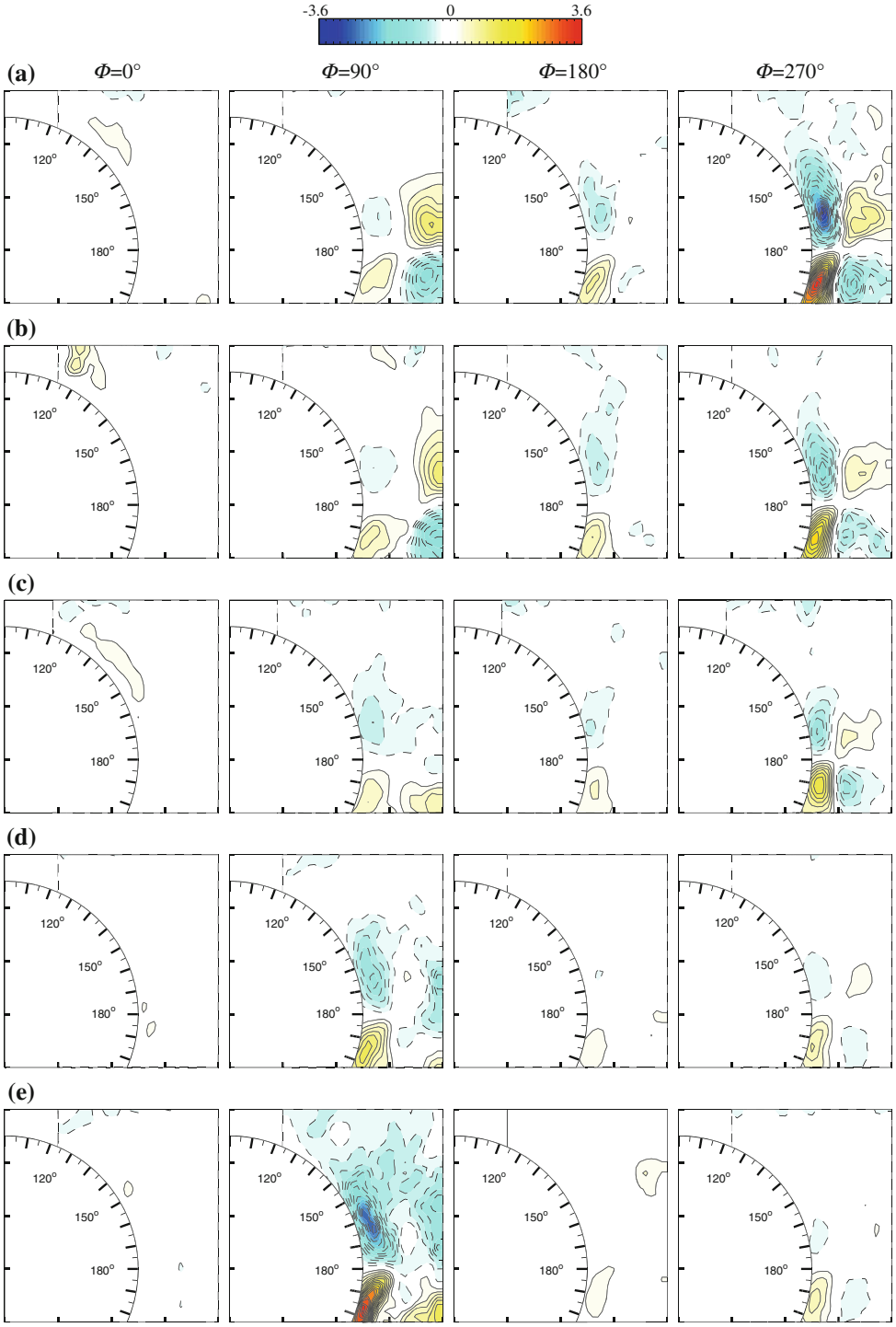

Fig. 14 Distributions of the phase-averaged vertical velocity gradient in the near-wake region. The x-axis is from $x/D = 0$ to $x/D = 0.8$, and the y-axis is from $y/D = -0.2$ to $y/D = 0.6$. **a** $k = 0.25$, **b** 0.50, **c** 1.00, **d** 2.00, **e** 4.00. Contour levels: ± 0.2

the separation point, similar with Jukes and Choi's (2009b) method, which might be worthy of further investigation.

The present experiment was conducted only at one excitation frequency and one Reynolds number. However, based on a series of investigations (Feng and Wang 2010; Feng et al. 2010, 2011; and this study), it is suggested that a considerable control effect at other excitation frequencies or much higher Reynolds numbers can also be achieved if only the strength of the synthetic jet vortex pair is enhanced. This can be done by increasing either of the excitation amplitude, excitation frequency, or suction duty cycle factor, or all of them.

Acknowledgments This work has been supported by the National Natural Science Foundation of China (No. 10832001 and No. 50976007).

References

Akilli H, Sahin B, Tumen NF (2005) Suppression of vortex shedding of circular cylinder in shallow water by a splitter plate. Flow Meas Instrum 16(4):211–219

Akilli H, Karakus C, Akar A, Sahin B, Tumen NF (2008) Control of vortex shedding of circular cylinder in shallow water flow using an attached splitter plate. ASME J Fluids Eng 130(4):041401

Amitay M, Honohan A, Trautman M, Glezer A (1997) Modification of the aerodynamic characteristics of bluff bodies using fluidic actuators. AIAA paper 97-2004

Amitay M, Smith BL, Glezer A (1998) Aerodynamic flow control using synthetic jet technology. AIAA paper 98-0208

Antonia RA, Rajagopalan S (1990) Determination of drag of a circular cylinder. AIAA J 28(10):1833–1834

Baek H, Karniadakis GE (2009) Suppressing vortex-induced vibrations via passive means. J Fluids Struct 25(5):848–866

Benard N, Balcon N, Touchard G, Moreau E (2008) Control of diffuser jet flow: turbulent kinetic energy and jet spreading enhancements assisted by a non-thermal plasma discharge. Exp Fluids 45(2):333–355

Béra JC, Michard M, Sunyach M, Comte-Bellot G (2000) Changing lift and drag by jet oscillation: experiments on a circular cylinder with turbulent separation. Eur J Mech B/Fluids 19(5):575–595

Cantwell B, Coles D (1983) An experimental study of entrainment and transport in the turbulent near wake of a circular cylinder. J Fluid Mech 136:321–374

Crook A, Sadri AM, Wood NJ (1999) The development and implementation of synthetic jets for the control of separated flow. AIAA paper 99-3176

Feng LH, Wang JJ (2010) Circular cylinder vortex-synchronization control with a synthetic jet positioned at the rear stagnation point. J Fluid Mech 662:232–259

Feng LH, Wang JJ, Xu CJ (2008) Experimental verification of a novel actuator signal for efficient synthetic jet. J Exp Fluid Mech 22(1):6–10 (in Chinese)

Feng LH, Wang JJ, Pan C (2010) Effect of novel synthetic jet on wake vortex shedding modes of a circular cylinder. J Fluids Struct 26(6):900–917

Feng LH, Wang JJ, Pan C (2011) Proper orthogonal decomposition analysis of vortex dynamics of a circular cylinder under synthetic jet control. Phys Fluids 23(1):014106

Fu H, Rockwell D (2005) Shallow flow past a cylinder: control of the near wake. J Fluid Mech 539:1–24

Fujisawa N, Takeda G (2003) Flow control around a circular cylinder by internal acoustic excitation. J Fluids Struct 17(7):903–913

Fujisawa N, Takeda G, Ike N (2004) Phase-averaged characteristics of flow around a circular cylinder under acoustic excitation control. J Fluids Struct 19(2):159–170

Fujisawa N, Tanahashi S, Srinivas K (2005) Evaluation of pressure field and fluid forces on a circular cylinder with and without rotational oscillation using velocity data from PIV measurement. Meas Sci Technol 16(4):989–996

Glezer A, Amitay M (2002) Synthetic jets. Annu Rev Fluid Mech 34:503–529

Glezer A, Amitay M, Honohan AM (2003) Aspects of low- and high-frequency aerodynamic flow control. AIAA paper 2003-0533

Grinstein FF (2001) Vortex dynamics and entrainment in rectangular free jets. J Fluid Mech 437:69–101

Holman R, Utturkar Y, Mittal R, Smith BL, Cattafesta L (2005) Formation criterion for synthetic jets. AIAA J 43(10):2110–2116

Hwang JY, Yang KS, Sun SH (2003) Reduction of flow-induced forces on a circular cylinder using a detached splitter plate. Phys Fluids 15(8):2433–2436

Jukes TN, Choi K-S (2009a) Flow control around a circular cylinder using pulsed dielectric barrier discharge surface plasma. Phys Fluids 21(8):084103

Jukes TN, Choi K-S (2009b) Long lasting modifications to vortex shedding using a short plasma excitation. Phys Rev Lett 102(25):254501

Kim W, Yoo JY, Sung J (2006) Dynamics of vortex lock-on in a perturbed cylinder wake. Phys Fluids 18(7):074103

Konstantinidis E, Balabani S (2007) Symmetric vortex shedding in the near wake of a circular cylinder due to streamwise perturbations. J Fluids Struct 23(7):1047–1063

Lam K, Wang FH, So RMC (2004) Three-dimensional nature of vortices in the near wake of a wavy cylinder. J Fluids Struct 19(6):815–833

Mittal S (2003) Effect of a "slip" splitter plate on vortex shedding from a cylinder. Phys Fluids 15(3):817–820

Rediniotis OK, Ko J, Yue X, Kurdila AJ (1999) Synthetic jets, their reduced order modeling and applications to flow control. AIAA paper 99-1000

Rumsey CL, Gatski TB, Sellers III WL, Vatsa VN, Viken S (2004) Summary of the 2004 CFD validation workshop on synthetic jets and turbulent separation control. AIAA paper 2004-2217

Shan RQ, Wang JJ (2010) Experimental studies of the influence of parameters on axisymmetric synthetic jets. Sensor Actuat A Phys 157(1):107–112

Smith BL, Glezer A (1998) The formation and evolution of synthetic jets. Phys Fluids 10(9):2281–2297

Smith BL, Swift GW (2003) A comparison between synthetic jets and continuous jets. Exp Fluids 34(4):467–472

So RMC, Zhou Y, Liu MH (2000) Free vibrations of an elastic cylinder in a cross flow and their effects on the near wake. Exp Fluids 29(2):130–144

Spall RE, Anderson EA, Allen J (2004) Momentum flux in plane, parallel jets. ASME J Fluids Eng 126(4):665–670

Tan GK, Wang JJ, Li QS (2001) Drag reduction technique of cylinder and mechanism research. J Beijing Univ Aeronaut Astrol 27(6):658–661 (in Chinese)

Tensi J, Boué I, Paillé F, Dury G (2002) Modification of the wake behind a circular cylinder by using synthetic jets. J Vis 5(1):37–44

Toyoda K, Hiramoto R (2009) Manipulation of vortex rings for flow control. Fluid Dyn Res 41(5):051402

van Dam CP (1999) Recent experience with different methods of drag prediction. Prog Aerosp Sci 35(8):751–798

Wang JJ, Feng LH, Xu CJ (2007) Experimental investigations on separation control and flow structure around a circular cylinder with synthetic jet. Sci China Ser E 50(5):550–559

Wang JJ, Shan RQ, Zhang C, Feng LH (2010) Experimental investigation of a novel two-dimensional synthetic jet. Eur J Mech B/Fluids 29(5):342–350

Wolfe D, Ziada S (2003) Feedback control of vortex shedding from two tandem cylinders. J Fluids Struct 7(4):579–592

Yannopoulos PC (2006) An improved integral model for plane and round turbulent buoyant jets. J Fluid Mech 547:267–296

Zdravkovich MM (1997) Flow around circular cylinders, fundamentals, vol 1. Oxford University Press, Oxford

Zhang PF, Wang JJ (2007) Novel signal wave pattern for efficient synthetic jet generation. AIAA J 45(5):1058–1065

Zhang MM, Cheng L, Zhou Y (2004) Closed-loop-controlled vortex shedding and vibration of a flexibly supported square cylinder under different schemes. Phys Fluids 16(5):1439–1448

Zhang PF, Wang JJ, Feng LH (2008) Review of zero-net-mass-flux jet and its application in separation flow control. Sci China Ser E 51(9):1315–1344

Zhou Y, Yiu MW (2006) Flow structure, momentum and heat transport in a two-tandem cylinder wake. J Fluid Mech 548:17–48

Zhou Y, Alam MM, Yang HX, Guo H, Wood DH (2011) Fluid forces on a very low Reynolds number airfoil and their prediction. Int J Heat Fluid Flow 32(1):329–339